ACS APPLIED MATERIALS & INTERFACES

Research Article

Cite This: ACS Appl. Mater. Interfaces 2019, 11, 26144−26151

www.acsami.org

Rational Molecular Design of Dibenzo[*a*,*c*]phenazine-Based Thermally Activated Delayed Fluorescence Emitters for Orange-Red OLEDs with EQE up to 22.0%

Feng-Ming Xie,[†] Hao-Ze Li,[†] Guo-Liang Dai,[†] Yan-Qing Li,[‡] Tao Cheng,[‡] Miao Xie,[‡] Jian-Xin Tang,*[,‡] and Xin Zhao*[,†]

[†]College of Chemistry, Biology and Material Engineering, Suzhou University of Science and Technology, Suzhou 215009, P. R. China

[‡]Institute of Functional Nano & Soft Materials (FUNSOM), Jiangsu Key Laboratory for Carbon-Based Functional Materials & Devices, Soochow University, Suzhou 215123, P. R. China

Supporting Information

ABSTRACT: The design and synthesis of highly efficient thermally activated delayed fluorescence (TADF) emitters with an electroluminescence wavelength beyond 600 nm remains a great challenge for organic light-emitting diodes (OLEDs). To solve this issue, three TADF molecules, *x*DMAC−BP (*x* = 1, 2, 3), are developed in combination with the rigid planar dibenzo[*a*,*c*]phenazine (BP) acceptor core and different numbers of 9,9-dimethylacridan (DMAC) donors. All these emitters possess stable internal charge transfer and a large dihedral angle between the donors and planar BP core. The emission wavelength can be regulated from 541 to 605 nm by increasing the number of the donor DMAC units because of the controllable tuning of the intramolecular charge transfer effect and the molecular geometrical structure. The photoluminescence quantum yields of these emitters are improved from 42 to 89% with the increase in the number of DMAC units. The orange-red OLEDs employing the *x*DMAC−BP emitters exhibit maximum external quantum efficiency (EQE) of 22.0% at 606 nm, which is the highest EQE of the previously reported TADF OLEDs exceeding 600 nm.

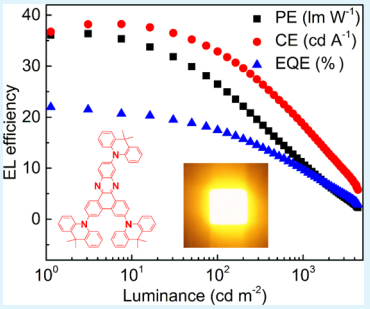

KEYWORDS: *thermally activated delayed fluorescence, dibenzo[a,c]phenazine derivatives, intramolecular charge transfer, orange-red emission, organic light emitting diodes*

1. INTRODUCTION

Organic light emitting diodes (OLEDs) have been attracting much attention owing to their numerous applications as solid-state lighting sources and display.[1−5] The internal quantum efficiency (IQE) of OLEDs using first-generation fluorescent materials is limited to 25% for the reason that the emitter can only harvest singlet excitons.[6−8] The phosphorescent materials that contain noble-metal atoms can fully utilize both singlet and triplet excitons through effective spin−orbital coupling, achieving an IQE of ∼100%.[9] However, some disadvantages such as expensive material cost and short lifetime hinder the extension of phosphorescent materials.[10−12] After the pioneering research by Adachi et al.,[13] thermally activated delayed fluorescence (TADF) material has drawn great attraction in recent years,[14] which show potential as an interesting low-cost alternative to phosphorescent materials.[15,16] The TADF emitters can reach 100% IQE by converting all singlet and triplet excitons into photons via the reverse intersystem crossing (RISC) process from the lowest triplet excited state (T_1) to singlet excited state (S_1).[17−22] A sufficiently small S_1−T_1 energy split (ΔE_{ST}) is necessary for the efficient RISC process.[2] Generally, such a small ΔE_{ST} can be achieved by constructing a twisted donor−acceptor structure with adequate separation between the highest occupied molecular orbital (HOMO) and the lowest unoccupied molecular orbital (LUMO).[23,24]

To date, tremendous advance has occurred on TADF emitters. For example, TADF OLEDs have reached the external quantum efficiency (EQE) of ∼37% for sky-blue emission[25] and over 37% for green emission,[6] respectively. Nevertheless, the development of high-efficiency TADF OLEDs with orange-red/red emissions[26] is relatively backward, although they have wide applications in bioimaging, sensors, communications, and night vision.[20,27] The efficiency of orange-red/red TADF emitters is lower than those of blue and green emissions, and the EQEs of TADF-based OLEDs up to 20% with the electroluminescence (EL) peak exceeding 600 nm have rarely been reported. For example, Adachi's group demonstrated the TADF OLED with an EQE of 17.5% at 610 nm.[28] Furue et al. reported four efficient orange-red TADF emitters, leading to a maximum EQE of 20.0% and the EL peak at 617 nm for Da-CNBQx-based OLEDs.[29] Zeng et al. achieved the EQE of 21.0% with an EL peak at 600 nm by using a NAI−9,9-dimethylacridan (DMAC) emitter.[26] One of

Received: April 12, 2019
Accepted: June 19, 2019
Published: June 19, 2019

DOI: 10.1021/acsami.9b06401
ACS Appl. Mater. Interfaces 2019, 11, 26144−26151

Scheme 1. Synthetic Routes of the Three Compounds

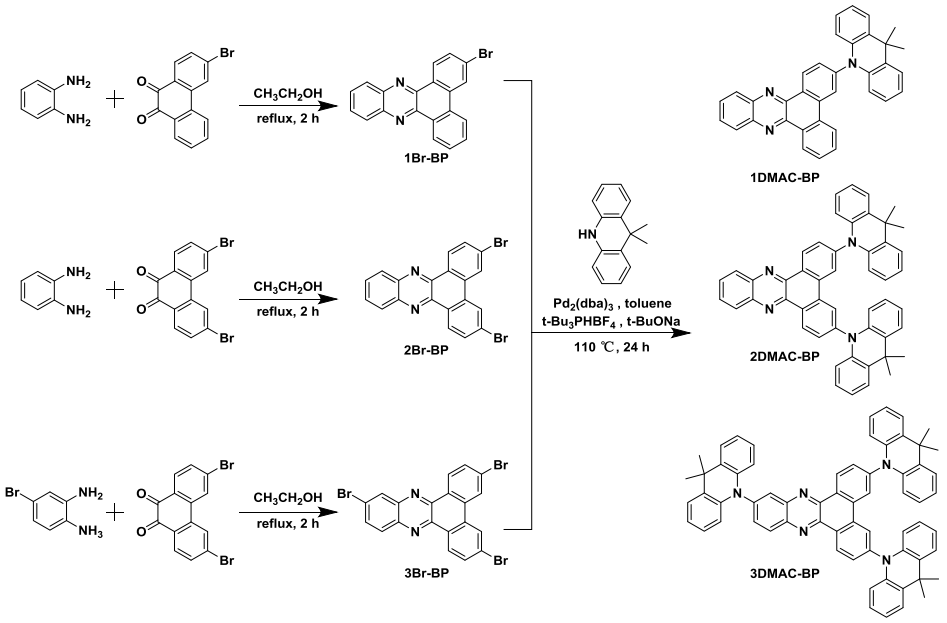

the main challenges in achieving highly efficient orange-red TADF materials is to simultaneously realize a small ΔE_{ST} and a high photoluminescence quantum yield (PLQY) through the rational molecular design. According to the energy-gap theory, the PLQY values tend to decrease with respect to the increase in the emission wavelength for long-wavelength TADF emitters.[26,30−33] Hence, the molecular design and synthesis of orange-red/red TADF emitters with EQE > 20% and EL emission wavelength longer than 600 nm remain as a great challenge.

In this paper, high-efficiency long-wavelength TADF materials have been demonstrated through the method: (i) the dibenzo[*a*,*c*]phenazine (BP) unit with high rigidity and coplanar π-conjugated structure is employed as an acceptor core, which favors the reduction of the band gap and thereby the emission red-shift. (ii) Various amounts of DMAC are used as a donor by adding to the 3, 6, and 11 positions of the BP core to construct a series of *x*DMAC−BP (*x* = 1, 2, 3) TADF materials, which could strengthen the intramolecular charge transfer (ICT) intensity by increasing the number of DMAC donors. (iii) The *x*DMAC−BP (*x* = 1, 2, 3) molecular structure with a typical twisted ICT state enables the simultaneous realization of long-wavelength emission, small ΔE_{ST}, and high PLQY. Consequently, the emission colors of *x*DMAC−BP (*x* = 1, 2, 3) can be effectively tuned from green to orange-red when the number of the DMAC donor units is changed to regulate the ICT effect. The PLQYs of these emitters are significantly improved from 42 to 89% as the number of DMAC units increased. The orange-red OLEDs employing the 3DMAC−BP emitters show a maximum EQE of 22.0% with an EL peak at 606 nm, which is the highest value among previously reported TADF OLEDs exceeding 600 nm.

2. EXPERIMENTAL SECTION

2.1. Synthesis and Device Fabrication. All the materials were purchased without further purification. Details of the synthesis procedure are shown in Scheme 1 and Supporting Information. OLEDs were fabricated on the ITO-coated glass substrates. Ultrasonic cleaning of the ITO-coated glass substrate was performed with deionized water, ethanol, and acetone and then dried in an oven at 110 °C. After the UV−ozone treatment for 15 min, ITO-coated glass substrates were transferred into a high-vacuum evaporation chamber with a high vacuum $\lesssim 2 \times 10^{-4}$ Pa for the deposition of organic materials and metal electrodes with a shadow mask. MoO_3 was used as a hole-injection layer, NPB was employed as a hole-transport layer, TCTA was employed as an electron/exciton-blocking layer, mCBP was employed as the host material, TmPYPB was employed as an electron-transport/hole-blocking layer, and LiF/Al was used as a bilayer cathode. The active area was determined to be 0.1 cm^2. Deposition rates were 0.1−0.2 Å/s for MoO_3, 2−3 Å/s for organic materials (expect for ∼1 Å/s for the host and ∼0.2 Å/s for TADF emitters), 0.1 Å/s for LiF layer, and >6 Å/s for Al, respectively.

2.2. Materials Characterization. ^{1}H NMR and ^{13}C NMR were recorded with Germany Bruker AVANCE III type NMR spectrometer in $CDCl_3$ solution (see Figures S1−S6). Mass spectra were measured on a GCT Premier type [electron bombardment (EI)−high-resolution time-of-flight (TOF)] mass spectrometer (see Figures S7 and S8). Matrix-assisted laser desorption/ionization TOF (MALDI-TOF) mass spectroscopy was acquired on an ultrafleXtreme MALDI-TOF mass spectrometer with a 1 kHz smart beam-II laser (see Figure S9). Elemental analysis test was done using Vario Micro cube elemental analyzer. The absorption spectra were recorded with a LAMBDA 750 UV−vis spectrophotometer. The fluorescence spectra were measured with a FM-4 type fluorescence spectrophotometer (JY Company, French). The low-temperature phosphorescence spectra were measured with a FLS 920 spectrometer (Edinburgh Corporation) by using toluene as a solvent at 77 K. Transient PL spectra were measured with fluorescence lifetime spectrometer C11367 series (Quantaurus-Tau). PLQYs were obtained by using a C9920-02G type fluorescence spectrophotometer (Hamamatsu, Japan) with an integrating sphere at room temperature (RT) in a nitrogen atmosphere. Cyclic voltammetry (CV) measurements were conducted on a RST 3100 electrochemical work station. Thermal gravimetric analysis (TGA) was conducted with a HCT-2 instrument. Differential scanning calorimetry (DSC) was performed on a Pyris Diamond DSC thermal analyzer. EL characteristics of OLEDs were examined simultaneously with a computer-controlled programmable power source (Keithley model 2400) and a luminance meter/spectrometer (Photo Research PR655).

3. RESULT AND DISCUSSION

In order to investigate the geometrical structures and electronic properties of three BP derivatives (i.e., 1DMAC−

DOI: 10.1021/acsami.9b06401
ACS Appl. Mater. Interfaces 2019, 11, 26144−26151

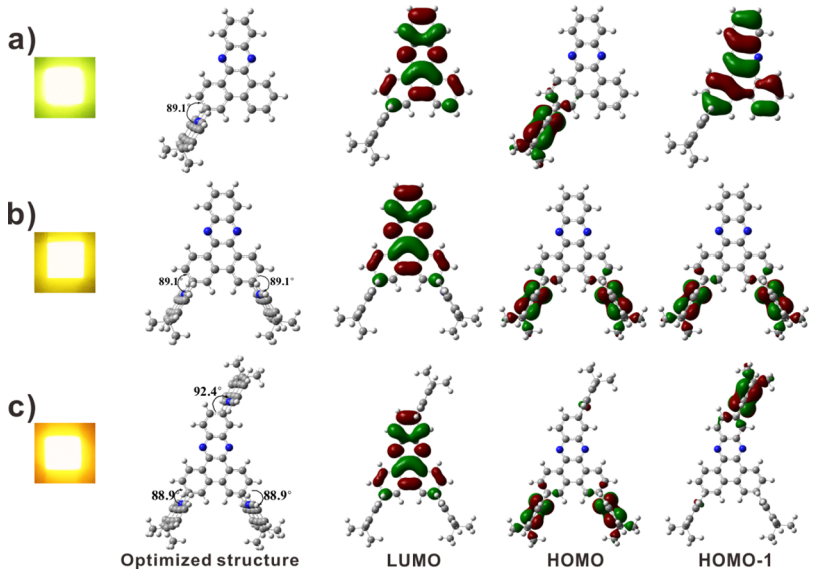

Figure 1. Emission color, optimized structure, and density-of-state distributions of LUMO/HOMO/HOMO − 1 of (a) 1DMAC−BP, (b) 2DMAC−BP, and (c) 3DMAC−BP, respectively.

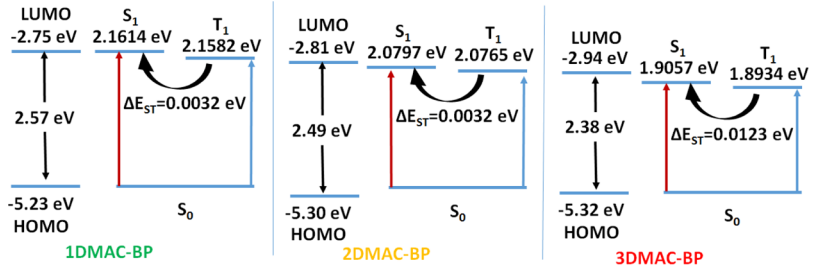

Figure 2. Calculated energy levels of 1DMAC−BP, 2DMAC−BP, and 3DMAC−BP.

Table 1. Summary of Photophysical, Electrochemical, and Thermal Properties of All Compounds

compound	λ_{abs} [a] [nm]	$\lambda_{Fl.}$ [b] [nm]	$\lambda_{Ph.}$ [c] [nm]	PLQY[d] [%]	PLQY[e] [%]	fwhm[f] [nm]	T_d [g] [°C]	ΔE_{ST} [h] [eV]	E_g [i] [eV]	HOMO/LUMO[j] [eV]
1DMAC−BP	382	541	545	22	42	83	378	0.22	2.62	−5.01/−2.39
2DMAC−BP	380	553	549	40	84	98	399	0.21	2.49	−4.98/−2.49
3DMAC−BP	386/456	605	595	44	89	97	413	0.05	2.35	−4.99/−2.64

[a]In toluene. [b]Fluorescent emission peak. [c]First phosphorescence emission peak. [d]PLQY for neat films. [e]PLQY for doped films. [f]fwhm of the fluorescence spectra. [g]Decomposition temperature (T_d) with 5% weight loss. [h]$\Delta E_{ST} = E_S - E_T$. [i]$E_g = 1240/\lambda_{onset}$. [j]The HOMO levels were determined from the onsets of the oxidation potential of CV, $E_{LUMO} = E_g + E_{HOMO}$.

BP, 2DMAC−BP, and 3DMAC−BP), density functional theory (DFT) and time-dependent DFT calculations were performed using the Gaussian 09 program package with the B3LYP/6-311+G* method.[33,34] Figure 1 displays the optimized structure and the density-of-state distributions of LUMO, HOMO, and HOMO − 1 levels of the BP derivatives. These three molecules show large dihedral angle of ∼90° between the DMAC donors of different substituted bits and the planar BP acceptor unit in the optimized geometries. Moreover, there is a large separation between LUMO and HOMO/HOMO − 1 in these molecules. As shown in Figure 1, the LUMO level of each compound was found to be completely distributed over the central BP core, whereas the HOMO was mainly localized on the DMAC units with a slight extent on the adjacent benzene ring. In addition, the HOMO − 1 electronic cloud of 3DMAC−BP was mainly distributed on the DAMC unit of 11-position, implying that the HOMO − 1-to-LUMO transition with approximate energies is allowed.[33] Consistent with the large LUMO-to-HOMO separation and very pretwisted structures in these molecules, the theoretical ΔE_{ST} values of these three BP derivatives are very small (<0.02 eV) (Figure 2, Table S1). The results will be favorable for the RISC process and conducive to obtaining a high PLQY.

The photophysical, electrochemistry and thermal properties of the three compounds are summarized in Table 1. Figure 3 shows the UV−vis and PL spectra of three BP derivatives, which were measured in toluene at RT. It is evident that there is a wide wavelength scale of CT bands in all the three compounds.[12] The lower absorption band at the wavelength longer than 410 nm can be attributed to the ICT from the DMAC donors to the BP core. In addition, the CT band is broadened with respect to the increase in the number of DMAC units, indicating that the ICT state becomes more stable for the presence of more DMAC donors. These emitters exhibit a wide range from green to orange-red bands in PL spectra with the peaks at 541, 553, and 605 nm for 1DMAC−

DOI: 10.1021/acsami.9b06401
ACS Appl. Mater. Interfaces 2019, 11, 26144−26151

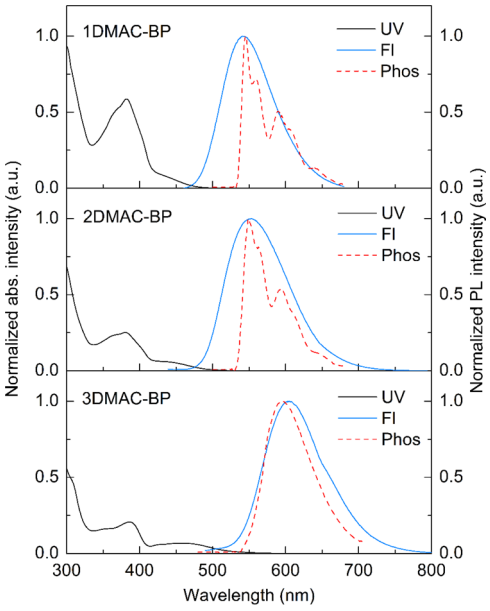

Figure 3. Normalized UV−vis and PL spectra of 1DMAC−BP, 2DMAC−BP, and 3DMAC−BP in toluene.

BP, 2DMAC−BP, and 3DMAC−BP, respectively. These peaks arise from the ^{1}CT (singlet charge transfer state) emission. Compared with 1DMAC−BP and 2DMAC−BP, an obvious red-shift of more than 50 nm is noted for the PL spectrum of 3DMAC−BP because of the stronger ICT ability of tri-donors. Correspondingly, the 2DMAC−BP exhibits a slight red-shift of 12 nm relative to that of 1DMAC−BP because of the use of one more acridine donor. These results indicate that the 3DMAC−BP with a star-shaped molecular configuration may possess the strong ICT effect.

The phosphorescence spectra of three emitters were recorded in toluene at 77 K. As shown in Figure 3, the S_1 and T_1 values can be estimated from the onset wavelengths of the fluorescence and phosphorescence spectra,[26] respectively. 1DMAC−BP and 2DMAC−BP possess the similar S_1 levels of 2.54 and 2.52 eV, as well as the similar T_1 levels of 2.32 and 2.31 eV, respectively. On the contrary, 3DMAC−BP shows a lower S_1 (2.31 eV) and T_1 (2.26 eV) than those of 1DMAC−BP and 2DMAC−BP, which can be attributed to the stronger ICT between the BP accepter core and tri-donor moieties (particularly, from 11-position donor). The ΔE_{ST} values can be calculated from the energy level of S_1 and T_1, revealing the results of 0.22, 0.21, and 0.05 eV for 1DMAC−BP, 2DMAC−BP, and 3DMAC−BP, respectively. A high TADF efficiency in BP derivatives is thus expected because of such small ΔE_{ST} values. Especially, the ΔE_{ST} of 3DMAC−BP (~0.05 eV) is quite tiny, which is very conducive to the efficient RISC process.

The HOMO and LUMO energy levels of three emitters were obtained in the DCM solution using CV measurements. As depicted in Figure 4a, all these molecules show two pairs reversible oxidation/reduction potentials, testifying good electrochemical stability.[35] As estimated from the onset of oxidation potentials, these emitters have similar HOMO levels of ~5.0 eV. The LUMO levels reveal a decrease with an increase in the number of DMAC, which is ascribed to the more electron-donating DMAC moieties and stronger ICT effect. Consequently, it is clear that the HOMO−LUMO energy gaps of three emitters gradually decreased with an

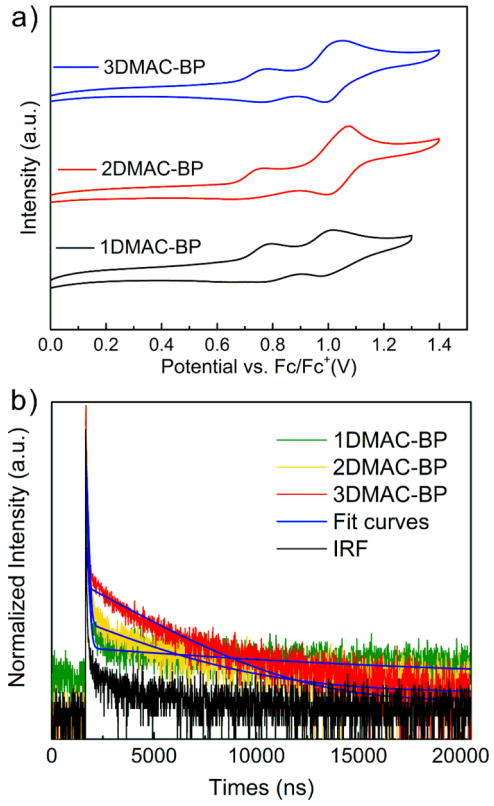

Figure 4. (a) Cyclic voltammogram of target compounds in CH_2Cl_2 (10^{-5} M). (b) Transient PL decay curves of 20 wt % BP derivatives doped into mCBP films.

increase in the number of DMAC donors, which are consistent with the red-shift of the PL spectra as shown in Figure 3. In addition, the relatively lower LUMO levels may easily cause electroplex interactions with a shallow HOMO level of the adjacent hole-transporting layer.[12] Meanwhile, both HOMO and LUMO levels of these three emitters match well with the conventional hole-transporting and electron-transporting materials, facilitating charge injection from the adjacent layers.[35] At the same time, the TGA measurements (Figure S10a) indicate that three emitters have high decomposition temperatures (T_d, 5% weight loss), such as 378 °C for 1DMAC−BP, 399 °C for 2DMAC−BP, and 413 °C for 3DMAC−BP (Table 1). The glass transition temperature (T_g) for each compound was not observed from the DSC measurements (Figure S10b). These results indicate that all these three emitters have superior thermal stability for the OLED fabrication via vacuum thermal deposition.

To clarify the TADF nature and gain deep insight in the structure−property relationships of these materials, transient PL characters of the doped films (20 wt % *x*DMAC−BP doped into mCBP) were examined at RT. Figure 4b displays the transient PL decay spectra of three materials, which contain two components of a nanosecond-scale and a microsecond-scale. The prompt/delayed fluorescence lifetimes are 68 ns/12.6 μs for 1DMAC−BP, 58 ns/7.5 μs for 2DMAC−BP, and 32 ns/2.9 μs for 3DMAC−BP. A microsecond-scale decay lifetime reveals that three emitters can harvest T_1 excitons through the RISC process ($T_1 \rightarrow S_1 \rightarrow S_0$) rather than the radiation decay of traditional fluorescent materials ($S_1 \rightarrow S_0$), indicating that these emitters possess distinct TADF characteristics. Particularly, 3DMAC−BP has the shortest delayed

DOI: 10.1021/acsami.9b06401
ACS Appl. Mater. Interfaces 2019, 11, 26144−26151

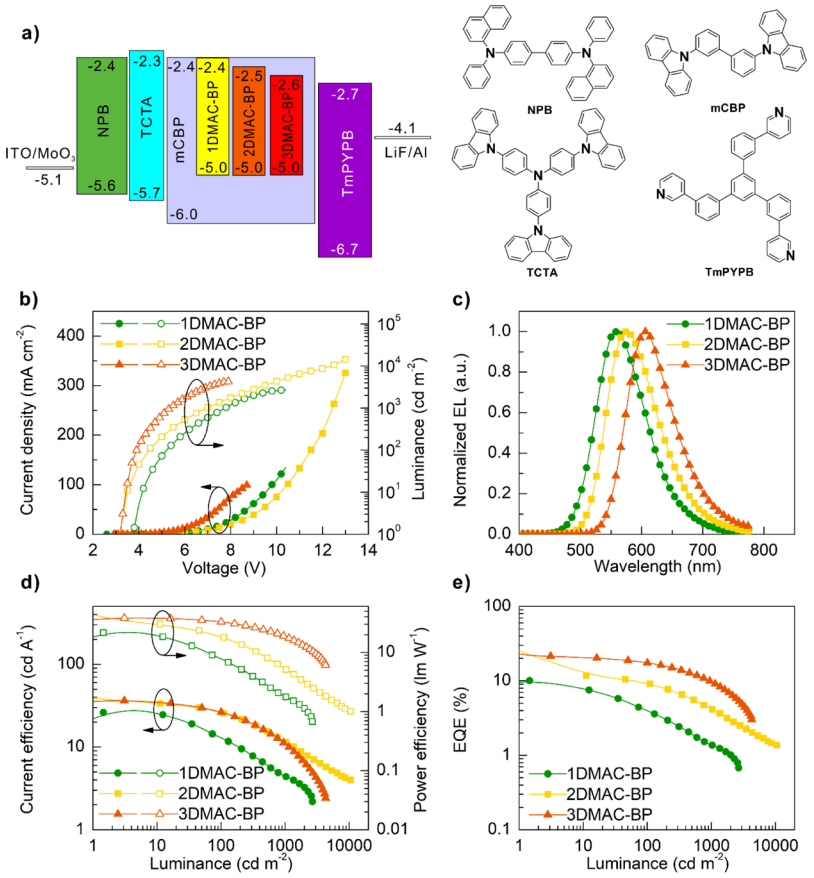

Figure 5. (a) Energy-level diagram and molecular structures employed in the devices. (b) Current density−voltage−luminance characteristics. (c) EL spectra of the devices. (d) CE and PE as a function of luminance. (e) EQE as a function of luminance.

Table 2. Performance Summary of OLEDs Using 1DMAC−BP, 2DMAC−BP, and 3DMAC−BP as Dopants, Respectively

device[a]	V_{on}[b] [V]	L[c] [cd]	PE[d] [lm W^{-1}]	CE[e] [cd A^{-1}]	EQE[f] [%]	λ_{EL}[g] [nm]	fwhm[h] [nm]	CIE[i] (x, y)
1DMAC−BP	3.7	2728	22.4	28.5	10.1/4.0/1.5	560	94	(0.43, 0.54)
2DMAC−BP	3.1	14 350	30.2	33.7	11.8/9.3/4.3	576	96	(0.49, 0.49)
3DMAC−BP	3.1	4038	36.4	38.2	22.0/17.5/9.7	606	90	(0.58, 0.41)

[a]Device configuration: ITO/MoO_3 (5 nm)/NPB (40 nm)/TCTA (10 nm)/mCBP:TADF emitter (20 wt % for 1DMAC−BP and 2DMAC−BP, 18 wt % for 3DMAC−BP) (20 nm)/TmPYPB (40 nm)/LiF (1 nm)/Al (100 nm). [b]The V_{on} at a brightness of 1 cd m^{-2}. [c]Maximum luminance. [d]Maximum PE. [e]Maximum CE. [f]Maximum EQE, and values at 100 and 1000 cd m^{-2}. [g]The wavelength of the EL peak. [h]fwhm of the EL peak. [i]CIE 1931 coordinates.

fluorescence lifetime among these three emitters, which can be attributed to the smallest ΔE_{ST} for the rapid up-conversion of T_1 excitons to the S_1 state and thus the reduction of triplet−triplet-annihilation, singlet−triplet-annihilation and triplet−polaron-annihilation.[33,36] Moreover, we measured the temperature-dependent transient PL decays in doped mCBP films from 100 to 300 K (Figure S11). The delayed component intensity is intensified with the increase of temperature, demonstrating typical TADF characteristics.

As listed in Tables 1 and S2, the PLQYs of three materials in neat films at RT are determined to be 22% for 1DMAC−BP, 40% for 2DMAC−BP, and 44% for 3DMAC−BP, respectively. Compared with the neat films, the PLQYs of three TADF emitters doped in a mCBP host (20 wt %) are drastically enhanced, showing the values of 42, 84, and 89% for 1DMAC−BP, 2DMAC−BP, and 3DMAC−BP, respectively. Such an enhancement on PLQYs can be ascribed to the suppression of the nonradiative process and the reduction of the concentration quenching in the doped films. Moreover, 3DMAC−BP has the highest PLQY (89%) in the doped films among three emitters, which may arise from the smallest ΔE_{ST}, the shortest delayed fluorescence lifetime, and limited concentration quenching. As obtained from the molecular orbital distribution calculation in Figure 1, the introduction of one more DMAC at the 11-position of 3DMAC−BP with a star-shaped molecular configuration can efficiently improve the intermolecular aggregation state, like the effective restriction of the intermolecular $\pi-\pi$ stacking for efficient PLQYs. To further understand the radiative decay, nonradiative decay, and delayed fluorescence decay processes of these emitters, the radiative rate constant (k_r) of the $S_1 \rightarrow S_0$, nonradiative rate constant (k_{nr}), rate constants (k_{ISC}) of the $S_1 \rightarrow T_1$, and the rate constant (k_{RISC}) of the $T_1 \rightarrow S_1$ RISC were estimated. As summarized in Table S3, the k_rs/k_{RISC}s values are 0.9×10^6/5.53×10^5 s^{-1} for 1DMAC−BP, 3.9×10^6/4.74×10^5 s^{-1} for 2DMAC−BP, and 9.3×10^6/10.01×10^5 s^{-1} for 3DMAC−BP, respectively.[37] These results indicate that 3DMAC−BP possesses the highest PLQY and the maximum k_{RISC}, which

DOI: 10.1021/acsami.9b06401
ACS Appl. Mater. Interfaces 2019, 11, 26144−26151

suggest that 3DMAC−BP could achieve better electroluminescent performance.

The EL properties of the emitters were further investigated by the fabrication of OLEDs using 1DMAC−BP, 2DMAC−BP, and 3DMAC−BP as the dopant, respectively. These devices were constructed with a device structure: ITO/MoO_3 (5 nm)/NPB (40 nm)/TCTA (10 nm)/mCBP:TADF emitter (20 wt % for 1DMAC−BP and 2DMAC−BP, and 18 wt % for 3DMAC−BP) (20 nm)/TmPYPB (40 nm)/LiF (1 nm)/Al (100 nm). The details of the device fabrication are given in the Experimental Section. Figure 5a displays the energy-level diagram of the devices and chemical structures of the related materials. The device performances are shown in Figure 5b−e and summarized in Table 2. As shown in Figure 5b, all the devices exhibit low turn-on voltages, which are 3.7, 3.1, and 3.1 V for 1DMAC−BP, 2DMAC−BP, and 3DMAC−BP-based OLEDs, respectively. The maximum brightness of these three OLEDs are 2728, 14 350, and 4038 cd m^{-2}, respectively. The EL spectra of three devices (Figure 5c) show yellow-green to orange-red emission. The EL spectra of 1DMAC−BP- and 2DMAC−BP-based OLEDs exhibit a peak at 560 and 576 nm with a full width at half maximum (fwhm) of 94 and 96 nm, and the CIE 1931 coordinates (Figure S12) of (0.43, 0.54) and (0.49, 0.49), respectively. The EL spectrum of 3DMAC−BP-based OLED shows the orange-red emission with a peak at 606 nm with a fwhm of 90 nm and the CIE of (0.58, 0.41) (Figure S12). The 1DMAC−BP-based device gives the maximum power efficiency (PE), current efficiency (CE), and EQE of 22.4 lm W^{-1}, 28.5 cd A^{-1}, and 10.1%, respectively (see Table 2). Meanwhile, the 2DMAC−BP-based device shows higher efficiencies of 30.2 lm W^{-1}, 33.7 cd A^{-1}, and 11.8%, which may originate from higher PLQY of 2DMAC−BP. After optimizing the doping concentration of 3DMAC−BP in the mCBP host (Figure S13 and Table S4), the 3DMAC−BP-based device exhibits a great PE and CE value of 36.4 lm W^{-1} and 38.2 cd A^{-1} respectvely. Notably, this device shows excellent EQE up to 22.0% without any optical out-coupling technology. As compared to previously reported data (Figure 6 and Table S5),[26,28,29,33,38−40] a state-of-the-art EQE of 22.0% is among the highest values for the orange-red TADF OLEDs with an EL peak wavelength over 600 nm. More importantly, the EQE value of the 3DMAC−BP-based device can maintain at a level of 17.5% with a brightness of 100 cd m^{-2}, which are much higher than most of orange-red TADF OLEDs with an EL peak larger than 600 nm.

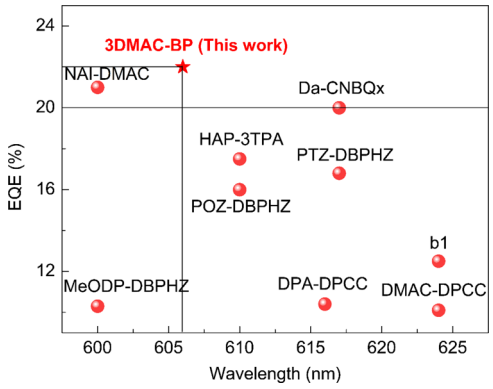

Figure 6. Comparison of high-efficiency orange-red TADF OLEDs reported in the literature with EQE ≥ 10.0% and EL peak wavelength ≥ 600 nm, which are taken from refs.[26,28,29,33,38,40]

4. CONCLUSIONS

In summary, we have designed and synthesized three twisted ICT-type TADF emitters, including 1DMAC−BP, 2DMAC−BP, and 3DMAC−BP with the rigid planar BP as the core and different numbers of DMAC as the donor. By tuning the ICT effect and molecular geometrical structure with the increase in the number of DMAC donors, the emission colors of these TADF emitters can be regulated from green to orange-red, and their PLQYs can be largely enhanced because of minimal ΔE_{ST} and high k_r. As a result, the orange-red OLEDs employing the TADF emitter of 3DMAC−BP show a maximum EQE of 22.0% with an EL peak at 606 nm, which is the highest among TADF-based OLEDs reported with the emission wavelength beyond 600 nm. These results provide an effective strategy for successfully designing and synthesizing high-performance TADF emitters with long-wavelength emission.

■ ASSOCIATED CONTENT

Supporting Information

The Supporting Information is available free of charge on the ACS Publications website at DOI: 10.1021/acsami.9b06401.

Photophysical characteristics of 1DMAC−BP, 2DMAC−BP, and 3DMAC−BP and device performances of 3DMAC−BP-based OLEDs (PDF)

■ AUTHOR INFORMATION

Corresponding Authors

*E-mail: jxtang@suda.edu.cn (J.-X.T.).
*E-mail: zhaoxin_sz@mail.usts.edu.cn (X.Z.).

ORCID

Jian-Xin Tang: 0000-0002-6813-0448
Xin Zhao: 0000-0002-4074-6056

Notes

The authors declare no competing financial interest.

■ ACKNOWLEDGMENTS

We acknowledge financial supports from the National Key R&D Program of China (no. 2016YFB0401002), the National Natural Science Foundation of China (grant 61520106012, 61705154).

■ REFERENCES

(1) Yu, L.; Wu, Z.; Xie, G.; Zeng, W.; Ma, D.; Yang, C. Molecular Design to Regulate the Photophysical Properties of Multifunctional TADF Emitters Towards High-Performance TADF-Based OLEDs with EQEs up to 22.4% and Small Efficiency Roll-offs. *Chem. Sci.* **2018**, *9*, 1385−1391.

(2) Huang, Z.; Xiang, S.; Zhang, Q.; Lv, X.; Ye, S.; Guo, R.; Wang, L. Highly Efficient Green Organic Light Emitting Diodes with Phenanthroimidazole-Based Thermally Activated Delayed Fluorescence Emitters. *J. Mater. Chem. C* **2018**, *6*, 2379−2386.

(3) Rajamalli, P.; Senthilkumar, N.; Gandeepan, P.; Huang, P.-Y.; Huang, M.-J.; Ren-Wu, C.-Z.; Yang, C.-Y.; Chiu, M.-J.; Chu, L.-K.; Lin, H.-W.; Cheng, C.-H. A New Molecular Design Based on Thermally Activated Delayed Fluorescence for Highly Efficient Organic Light Emitting Diodes. *J. Am. Chem. Soc.* **2016**, *138*, 628−634.

(4) Wada, Y.; Kubo, S.; Kaji, H. Adamantyl Substitution Strategy for Realizing Solution-Processable Thermally Stable Deep-Blue Ther-

DOI: 10.1021/acsami.9b06401
ACS Appl. Mater. Interfaces 2019, 11, 26144−26151

mally Activated Delayed Fluorescence Materials. *Adv. Mater.* **2018**, *30*, 1705641.
(5) Hatakeyama, T.; Shiren, K.; Nakajima, K.; Nomura, S.; Nakatsuka, S.; Kinoshita, K.; Ni, J.; Ono, Y.; Ikuta, T. Ultrapure Blue Thermally Activated Delayed Fluorescence Molecules: Efficient HOMO-LUMO Separation by the Multiple Resonance Effect. *Adv. Mater.* **2016**, *28*, 2777−2781.
(6) Wu, T.-L.; Huang, M.-J.; Lin, C.-C.; Huang, P.-Y.; Chou, T.-Y.; Chen-Cheng, R.-W.; Lin, H.-W.; Liu, R.-S.; Cheng, C.-H. Diboron Compound-Based Organic Light-Emitting Diodes with High Efficiency and Reduced Efficiency Roll-off. *Nat. Photonics* **2018**, *12*, 235−240.
(7) Kaji, H.; Suzuki, H.; Fukushima, T.; Shizu, K.; Suzuki, K.; Kubo, S.; Komino, T.; Oiwa, H.; Suzuki, F.; Wakamiya, A.; Murata, Y.; Adachi, C. Purely organic electroluminescent material realizing 100% conversion from electricity to light. *Nat. Commun.* **2015**, *6*, 8476.
(8) Liu, W.; Zheng, C.-J.; Wang, K.; Chen, Z.; Chen, D.-Y.; Li, F.; Ou, X.-M.; Dong, Y.-P.; Zhang, X.-H. Novel Carbazol-Pyridine-Carbonitrile Derivative as Excellent Blue Thermally Activated Delayed Fluorescence Emitter for Highly Efficient Organic Light-Emitting Devices. *ACS Appl. Mater. Interfaces* **2015**, *7*, 18930−18936.
(9) Kuei, C.-Y.; Tsai, W.; Tong, B.; Jiao, M.; Lee, W.; Chi, Y.; Wu, C.; Liu, S.; Lee, G.; Chou, P. Bis-Tridentate Ir(III) Complexes with Nearly Unitary RGB Phosphorescence and Organic Light-Emitting Diodes with External Quantum Efficiency Exceeding 31%. *Adv. Mater.* **2016**, *28*, 2795−2800.
(10) Mayr, C.; Lee, S. Y.; Schmidt, T. D.; Yasuda, T.; Adachi, C.; Brütting, W. Efficiency Enhancement of Organic Light-Emitting Diodes Incorporating a Highly Oriented Thermally Activated Delayed Fluorescence Emitter. *Adv. Funct. Mater.* **2014**, *24*, 5232−5239.
(11) Sohn, S.; Hyun Koh, B.; Baek, J. Y.; Chan Byun, H.; Lee, J. H.; Shin, D.-S.; Ahn, H.; Lee, H.-K.; Hwang, J.; Jung, S.; Kim, Y.-H. Synthesis and Characterization of Diphenylamine Derivative Containing Malononitrile for Thermally Activated Delayed Fluorescent Emitter. *Dyes Pigm.* **2017**, *140*, 14−21.
(12) Wang, Z.; Li, Y.; Cai, X.; Chen, D.; Xie, G.; Liu, K.; Wu, Y.-C.; Lo, C.-C.; Lien, A.; Cao, Y.; Su, S.-J. Structure-Performance Investigation of Thioxanthone Derivatives for Developing Color Tunable Highly Efficient Thermally Activated Delayed Fluorescence Emitters. *ACS Appl. Mater. Interfaces* **2016**, *8*, 8627−8636.
(13) Uoyama, H.; Goushi, K.; Shizu, K.; Nomura, H.; Adachi, C. Highly Efficient Organic Light-Emitting Diodes from Delayed Fluorescence. *Nature* **2012**, *492*, 234−238.
(14) Wang, Y.; Zhu, Y.; Xie, G.; Xue, Q.; Tao, C.; Le, Y.; Zhan, H.; Cheng, Y. Red Thermally Activated Delayed Fluorescence Polymers Containing 9H-Thioxanthen-9-one-10,10-Dioxide Acceptor Group as Pendant or Incorporated in Backbone. *Org. Electron.* **2018**, *59*, 406−413.
(15) Tanaka, H.; Shizu, K.; Nakanotani, H.; Adachi, C. Twisted Intramolecular Charge Transfer State for Long-Wavelength Thermally Activated Delayed Fluorescence. *Chem. Mater.* **2013**, *25*, 3766−3771.
(16) Guo, J.; Li, X.-L.; Nie, H.; Luo, W.; Hu, R.; Qin, A.; Zhao, Z.; Su, S.-J.; Tang, B. Z. Robust Luminescent Materials with Prominent Aggregation-Induced Emission and Thermally Activated Delayed Fluorescence for High-Performance Organic Light-Emitting Diodes. *Chem. Mater.* **2017**, *29*, 3623−3631.
(17) Chan, C.-Y.; Cui, L.-S.; Kim, J. U.; Nakanotani, H.; Adachi, C. Rational Molecular Design for Deep-Blue Thermally Activated Delayed Fluorescence Emitters. *Adv. Funct. Mater.* **2018**, *28*, 1706023.
(18) Park, H.-J.; Han, S. H.; Lee, J. Y.; Han, H.; Kim, E.-G. Managing Orientation of Nitrogens in Bipyrimidine-Based Thermally Activated Delayed Fluorescent Emitters to Suppress Nonradiative Mechanisms. *Chem. Mater.* **2018**, *30*, 3215−3222.
(19) Pashazadeh, R.; Pander, P.; Lazauskas, A.; Dias, F. B.; Grazulevicius, J. V. Multicolor Luminescence Switching and Controllable Thermally Activated Delayed Fluorescence Turn on/Turn off in Carbazole-Quinoxaline-Carbazole Triads. *J. Phys. Chem. Lett.* **2018**, *9*, 1172−1177.
(20) Kim, J. H.; Yun, J. H.; Lee, J. Y. Recent Progress of Highly Efficient Red and Near-Infrared Thermally Activated Delayed Fluorescent Emitters. *Adv. Opt. Mater.* **2018**, *6*, 1800255.
(21) Wang, H.; Xie, L.; Peng, Q.; Meng, L.; Wang, Y.; Yi, Y.; Wang, P. Novel Thermally Activated Delayed Fluorescence Materials-Thioxanthone Derivatives and Their Applications for Highly Efficient OLEDs. *Adv. Mater.* **2014**, *26*, 5198−5204.
(22) Zhang, Y.; Zhang, D.; Cai, M.; Li, Y.; Zhang, D.; Qiu, Y.; Duan, L. Towards highly efficient red thermally activated delayed fluorescence materials by the control of intra-molecular π-π stacking interactions. *Nanotechnology* **2016**, *27*, 094001.
(23) Grybauskaite-Kaminskiene, G.; Volyniuk, D.; Mimaite, V.; Bezvikonnyi, O.; Bucinskas, A.; Bagdziunas, G.; Grazulevicius, J. V. Aggregation-Enhanced Emission and Thermally Activated Delayed Fluorescence of Derivatives of 9-Phenyl-9H -Carbazole: Effects of Methoxy and tert-Butyl Substituents. *Chem.—Eur. J.* **2018**, *24*, 9581−9591.
(24) Wang, C.; Zhou, K.; Huang, S.; Zhang, Q. Toward an Accurate Description of Thermally Activated Delayed Fluorescence: Equal Importance of Electronic and Geometric Factors. *J. Phys. Chem. C* **2019**, *123*, 13869−13876.
(25) Lin, T.-A.; Chatterjee, T.; Tsai, W.-L.; Lee, W.-K.; Wu, M.-J.; Jiao, M.; Pan, K.-C.; Yi, C.-L.; Chung, C.-L.; Wong, K.-T.; Wu, C.-C. Sky-Blue Organic Light Emitting Diode with 37% External Quantum Efficiency Using Thermally Activated Delayed Fluorescence from Spiroacridine-Triazine Hybrid. *Adv. Mater.* **2016**, *28*, 6976−6983.
(26) Zeng, W.; Lai, H.; Lee, W.; Jiao, M.; Shiu, Y.; Zhong, C.; Gong, S.; Zhou, T.; Xie, G.; Sarma, M.; Wong, K.; Wu, C.; Yang, C. Achieving Nearly 30% External Quantum Efficiency for Orange-Red Organic Light Emitting Diodes by Employing Thermally Activated Delayed Fluorescence Emitters Composed of 1,8-Naphthalimide-Acridine Hybrids. *Adv. Mater.* **2018**, *30*, 1704961.
(27) Wang, S.; Yan, X.; Cheng, Z.; Zhang, H.; Liu, Y.; Wang, Y. Highly Efficient Near-Infrared Delayed Fluorescence Organic Light Emitting Diodes Using a Phenanthrene-Based Charge-Transfer Compound. *Angew. Chem., Int. Ed.* **2015**, *54*, 13068−13072.
(28) Li, J.; Nakagawa, T.; MacDonald, J.; Zhang, Q.; Nomura, H.; Miyazaki, H.; Adachi, C. Highly Efficient Organic Light-Emitting Diode Based on a Hidden Thermally Activated Delayed Fluorescence Channel in a Heptazine Derivative. *Adv. Mater.* **2013**, *25*, 3319−3323.
(29) Furue, R.; Matsuo, K.; Ashikari, Y.; Ooka, H.; Amanokura, N.; Yasuda, T. Highly Efficient Red-Orange Delayed Fluorescence Emitters Based on Strong π-Accepting Dibenzophenazine and Dibenzoquinoxaline Cores: toward a Rational Pure-Red OLED Design. *Adv. Opt. Mater.* **2018**, *6*, 1701147.
(30) Li, Y.; Li, X.-L.; Chen, D.; Cai, X.; Xie, G.; He, Z.; Wu, Y.; Lien, A.; Cao, Y.; Su, S. Design Strategy of Blue and Yellow Thermally Activated Delayed Fluorescence Emitters and Their All-Fluorescence White OLEDs with External Quantum Efficiency Beyond 20%. *Adv. Funct. Mater.* **2016**, *26*, 6904−6912.
(31) Im, Y.; Kim, M.; Cho, Y. J.; Seo, J.-A.; Yook, K. S.; Lee, J. Y. Molecular Design Strategy of Organic Thermally Activated Delayed Fluorescence Emitters. *Chem. Mater.* **2017**, *29*, 1946−1963.
(32) Li, C.; Duan, R.; Liang, B.; Han, G.; Wang, S.; Ye, K.; Liu, Y.; Yi, Y.; Wang, Y. Deep-Red to Near-Infrared Thermally Activated Delayed Fluorescence in Organic Solid Films and Electroluminescent Devices. *Angew. Chem., Int. Ed.* **2017**, *56*, 11525−11529.
(33) Zhang, Q.; Kuwabara, H.; Potscavage, W. J.; Huang, S.; Hatae, Y.; Shibata, T.; Adachi, C. Anthraquinone-Based Intramolecular Charge-Transfer Compounds: Computational Molecular Design, Thermally Activated Delayed Fluorescence, and Highly Efficient Red Electroluminescence. *J. Am. Chem. Soc.* **2014**, *136*, 18070−18081.
(34) Becke, A. D. A new mixing of Hartree−Fock and local density-functional theories. *J. Chem. Phys.* **1993**, *98*, 1372−1377.
(35) Zhang, D.; Song, X.; Cai, M.; Kaji, H.; Duan, L. Versatile Indolocarbazole-Isomer Derivatives as Highly Emissive Emitters and Ideal Hosts for Thermally Activated Delayed Fluorescent OLEDs with Alleviated Efficiency Roll-Off. *Adv. Mater.* **2018**, *30*, 1705406.

DOI: 10.1021/acsami.9b06401
ACS Appl. Mater. Interfaces 2019, 11, 26144−26151

(36) Xie, G.; Chen, D.; Li, X.; Cai, X.; Li, Y.; Chen, D.; Liu, K.; Zhang, Q.; Cao, Y.; Su, S.-J. Polarity-Tunable Host Materials and Their Applications in Thermally Activated Delayed Fluorescence Organic Light-Emitting Diodes. *ACS Appl. Mater. Interfaces* **2016**, *8*, 27920−27930.
(37) Goushi, K.; Yoshida, K.; Sato, K.; Adachi, C. Organic light-emitting diodes employing efficient reverse intersystem crossing for triplet-to-singlet state conversion. *Nat. Photonics* **2012**, *6*, 253−258.
(38) Data, P.; Pander, P.; Okazaki, M.; Takeda, Y.; Minakata, S.; Monkman, A. P. Dibenzo[a,j]phenazine-Cored Donor-Acceptor-Donor Compounds as Green-to-Red/NIR Thermally Activated Delayed Fluorescence Organic Light Emitters. *Angew. Chem., Int. Ed.* **2016**, *128*, 5833−5838.
(39) Okazaki, M.; Takeda, Y.; Data, P.; Pander, P.; Higginbotham, H.; Monkman, A. P.; Minakata, S. Thermally activated delayed fluorescent phenothiazine-dibenzo[a,j]phenazine-phenothiazine triads exhibiting tricolor-changing mechanochromic luminescence. *Chem. Sci.* **2017**, *8*, 2677−2686.
(40) Wang, S.; Cheng, Z.; Song, X.; Yan, X.; Ye, K.; Liu, Y.; Yang, G.; Wang, Y. Highly Efficient Long-Wavelength Thermally Activated Delayed Fluorescence OLEDs Based on Dicyanopyrazino Phenanthrene Derivatives. *ACS Appl. Mater. Interfaces* **2017**, *9*, 9892−9901.

DOI: 10.1021/acsami.9b06401
ACS Appl. Mater. Interfaces 2019, 11, 26144−26151